RSC Advances

PAPER

View Article Online
View Journal | View Issue

Cite this: *RSC Adv.*, 2017, **7**, 56463

Thermoplasmonic dissipation in gold nanoparticle–polyvinylpyrrolidone thin films†

Tyler V. Howard,‡[a] Jeremy R. Dunklin, ‡[b] Gregory T. Forcherio [c] and D. Keith Roper *[bc]

Thermal dissipation of plasmon energy from gold nanoparticles (AuNPs) dispersed in transparent polymers is important to biotherapeutics, optoelectronics, sensing, and chemical separations. This work assessed heat dissipated from power extinguished by 16 nm AuNPs with negligible Rayleigh scattering cross-sections dispersed into subwavelength, 70 nm polyvinylpyrrolidone (PVP) films at interparticle separations much less than the resonant wavelength. In contrast to super-wavelength films with particles at separations near the resonant wavelength, measured optical extinction and temperature increase per NP (°C per NP) decreased as AuNP concentration increased: °C per NP decreased 22% and optical extinction per NP decreased 35% as AuNP concentration increased from 1.01 to 5.06 × 10^{15} NP per cm^3. The trend and magnitude of measured values were consistent with those from *a priori* description of optical extinction per NP from Maxwell Garnett effective medium theory (EMT) and from coupled dipole approximation (CDA). Optical power extinguished by the films exhibited a trend and magnitude consistent with finite element analysis (FEA) of thermal dissipation from subwavelength films at particle separations of 130 to 76 nm. Comparing measured values with results from EMT, CDA, and FEA distinguished contributions to plasmon-resonant optical extinction and heat dissipation. These results support design and adaptive control of thermal dissipation from plasmonic films.

Received 5th April 2017
Accepted 4th December 2017

DOI: 10.1039/c7ra03892e

rsc.li/rsc-advances

I. Introduction

Plasmonic nanoparticles (NP) dispersed in transparent polymer dissipate heat *via* plasmon–phonon interactions influenced by irradiation intensity, NP morphology[1] and host environment.[2] Such interactions have an impact on the use of NP-containing polymer films in biomedical therapeutics,[3] chemical separations,[4] sensing,[5] solar cells[6] and optical interconnects.[7] Thermoplasmonic heating is an outcome of optical damping of resonant continuous-wave or pulsed irradiation of NP[8] that have negligible Rayleigh scattering cross sections which occurs by absorption.[9,10] Overall dissipation of absorbed energy *via* radiative, conductive and convective pathways has been characterized in colloidal suspensions,[11,12] on super-wavelength ceramic[13] and polymer[14] substrates, and in multi-phase[15] and open systems.[16] However, evaluation of correlated optical and thermal effects in NP-containing films of subwavelength thickness remains sparse. Gold (Au) NPs dispersed in super-wavelength thick polydimethylsiloxane (PDMS) films at separations near or greater than localized surface plasmon resonance (LSPR) wavelength absorbed more power as optical extinction increased with AuNP content, and dissipated more heat.[17] Sufficient accrual of heat is reported to reshape NP[18] or melt (evaporate) surrounding solids (liquids).[15,16,19] In contrast, AuNP in water-soluble, subwavelength polyvinylpyrrolidone (PVP) films at separations less than LSPR wavelength extinguished less power as AuNP content increased.[20] This work measured and evaluated the thermal signature of power absorbed by AuNP concentrated in subwavelength PVP films and its dissipation as heat, which has not been reported to date.

Optical activity of isolated subwavelength NP is described by the Mie solution to Maxwell's equations, from which scattering and absorption cross-sections, efficiencies, and intensity distributions can be determined.[8] Optical extinction by AuNPs in the Rayleigh regime, with negligible Mie scattering cross-section, is dominated by absorption[9,10] and is characterizable by Beer–Lambert law[21] for isolated particles[10] and colloid suspensions[22] in homogeneous dielectric environments. The coupled dipole approximation (CDA) extends Mie particle polarizability to multiple-NP systems and accounts for interparticle interactions.[23,24] Maxwell-Garnett effective medium theory (EMT) calculates the field induced by nanoscale inclusions randomly dispersed in a homogeneous media[25] and approximates its distortion by electrostatic interaction between inclusions to calculate a bulk dielectric function.[26] This has been extended to

[a]*Department of Physics & Engineering Physics, Southeast Missouri State University, Cape Girardeau, Missouri 63701, USA*

[b]*Ralph E. Martin Department of Chemical Engineering, University of Arkansas, Fayetteville, Arkansas 72701, USA. E-mail: dkroper@uark.edu; Fax: +1 479 575 7926; Tel: +1 479 575 6691*

[c]*MicroElectronics-Photonics Program, University of Arkansas, Fayetteville, Arkansas 72701, USA*

† Electronic supplementary information (ESI) available. See DOI: 10.1039/c7ra03892e

‡ Authors contributed equally.

anisotropic inclusions[27] and finite-sized aggregates.[28] The optical response of non-scattering NP may be determined using the Fresnel equations for geometric transmission and reflection.[29] A microscopic energy balance[12] links nano-optical extinction to thermal dissipation and dynamics of heating and cooling.[13,15,20,30] A compact one-dimensional (1D) form of this balance is extensible to quantify thermal dissipation in 3D multi-scale plasmonic systems using finite element analysis (FEA).[31,32] Comparing optically extinguished power determined by Mie theory and CDA with FEA estimates of power dissipation by NPs in subwavelength polymer films could improve design and integration into opto- and bio-electronic devices.[33,34]

This work measured and simulated values of thermal dissipation compared to corresponding optical extinction of homogeneous 16 nm AuNPs dispersed in 70 nm thick PVP films at interparticle separations much less than the LSPR wavelength for the first time. These subwavelength films exhibited higher values of optical extinction per unit thickness and mass-corrected temperature increase per incident power than previously reported NP-embedded media. The temperature increase per NP measured at thermal equilibrium trended downward as concentration increased from 1.01 to 5.06×10^{15} NP per cm^3, consistent with both measured resonant extinction per NP and with *a priori* estimates of extinction by EMT and CDA. The fraction of extinguished power observed to dissipate as heat increased with AuNP concentration, consistent with 3D finite element analysis (FEA) of subwavelength PVP films. Comparing measured values with results from EMT, CDA, and FEA distinguished measurable effects potentially attributable to lateral optical dispersion, plasmonic saturation, edge effects, or interfacial resistance.

II. Methods

A. Fabrication

Nanocomposite films comprised of AuNP and polyvinylpyrrolidone (PVP) were fabricated with isopropanol (IPA)-suspended AuNP diluted with PVP and spin-coated onto polished BK-7 glass. Initially, dried spherical AuNP of 16 ± 2 nm diameter, with PVP coating ≤4.4 nm (Econix Dried, Nanocomposix, San Diego, CA, USA; AuNP specifications are in ESI†) were suspended in IPA at 1 mg ml^{-1}. The stock dispersion contained 5.67 mg ml^{-1} of PVP, providing the highest AuNP concentration of 3.50×10^{15} NP per cm^3 in PVP. The stock was progressively diluted with IPA containing 5.67 mg ml^{-1} 40 000 Da PVP. Approximately 40 μL of each AuNP–PVP–IPA dispersion was pipetted onto 1 cm × 1 cm × 500 μm BK-7 glass slides and spun at 4000 rpm to create each subwavelength film. BK-7 glass was polished and treated in a Piranha solution (3 : 1 concentrated sulfuric acid to 30% hydrogen peroxide) to remove organic impurities and to hydroxylate the surface for improved wettability. Structural fragility of these films required that they be kept on the BK-7 glass for transmission UV-vis and thermographic analyses.

B. Optical characterization

Transmission UV-visible spectra were taken with a light microscope (Eclipse LV100, Nikon Instruments, Melville, NY, USA) coupled to a spectrometer (Shamrock 303i, Andor Technology, Belfast, UK). The magnitude of extinction maxima corresponding to LSPR was calculated relative to an 800 nm baseline to account for broadband contributions from the polymer matrix and/or underlying glass substrate. Reflection values of AuNP–PVP films were obtained using an integrating sphere (IS200-4, Thorlabs, Newton, New Jersey, USA) coupled with a halogen white light source (OSL2, Thorlabs, Newton, New Jersey, USA) and a spectrometer (AvaSpec-2048, Avantes, Broomfield, CO, USA) that was off-axis from the white light source. Samples were irradiated by the white light source, with the PVP film facing away from the white light source. The sample was tilted at a small angle to capture the reflection spectra.

C. AuNP–PVP film thickness determination

A thickness for AuNP–PVP films of 70 ± 7 nm ($N = 500$) was determined from cross sections obtained from tracing an atomic force microscope (Veeco Dimension 3100, Vecco, Plainview, NY, USA) tip over a scratch in the 5.06×10^{15} NP per cm^3 film that was made by a razor. Atomic force microscopy measurements were corroborated with surface profilometry (DekTak, Bruker, Billerica, MA) and Beer-Lambert's law.

D. Thermal characterization

Each AuNP–PVP nanocomposite film was resonantly irradiated with a fiber-coupled 532 nm diode-pumped solid state laser (MXL-FN-532, CNI, Changchung, CN) and its temperature profile was recorded with an infrared thermal camera (ICI 7320, P-Series, Beaumont, Texas). The experimental setup is shown in Scheme 1. Laser intensity was calculated to be 70 W cm^{-2}, based on a 800 mW incident power focused to a 1.2 mm $D4\sigma$ diameter spot size (measured at its focal point on sample). Light from the fiber-coupled laser was captured, diffused by a 10° ground glass diffuser, and focused onto the samples by two lenses. A Gaussian power distribution was output from the diffuser. More details regarding the optical setup, measurement of spot size, and power distribution are in ESI.† Each sample was mounted with the PVP film facing the thermal camera; tweezers were used to minimize heat conduction.

E. Theoretical description

Description of Maxwell Garnett effective medium theory (EMT) and coupled dipole approximation used in this work are detailed in ESI.† For EMT, values of complex relative permittivity (dielectric function) of Au and PVP were used to estimate film absorbance, as shown in ESI.† Finite element analysis (FEA) simulations utilized the heat transfer in solids module in version 5.2a of COMSOL Multiphysics (COMSOL, Stockholm, Sweden). Thermal equilibrium was simulated with an applied heat source that corresponded to laser irradiation for comparison with measured steady-state temperatures.[31] Radiative, conductive, and convective cooling boundary conditions were used to estimate the rate at which heat was transferred to the surrounding environment (air). Thermal diffusivity controlled the developed temperature profile within the AuNP–PVP

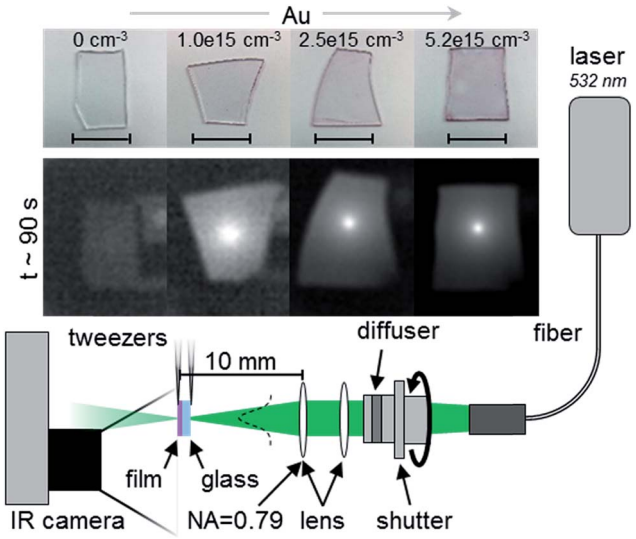

Scheme 1 Apparatus for thermal characterization of AuNP–PVP films shown in optical images (top row) and in infrared images captured at steady-state after approximately 90 seconds of irradiation (bottom row). Scale bar is equivalent to 1 cm. 10 mm scale bar in schematic is to indicate distance between focal point of last lens and focal point on sample. NA is the numerical aperture of the last lens.

nanocomposite media. Each AuNP–PVP film was approximated as a $10 \times 10 \times 7 \times 10^{-5}$ mm rectangular prism. Support BK-7 glass, measuring $10 \times 10 \times 0.5$ mm was immediately adjacent to the AuNP–PVP layer. A schematic of the model geometry used for these thermal simulations is shown in Scheme S1 in ESI.† Density and specific heat capacity values for each AuNP–PVP film were estimated as weighted averages of the pure material values, as shown in Table S1 in ESI.† Thermal conductivities used were 1.1 W mK^{-1} for glass and 0.27 W mK^{-1} for AuNP–PVP, respectively. The thermal conductivity of AuNP–PVP was assumed to be that of Au-free PVP, as mass fractions of metallic dispersions under 5% typically have negligible effect on bulk thermal conductivity.[35]

Plasmonic heating from laser irradiation was represented by a circular, radially uniform volumetric heat source with a diameter of 1.2 mm. This absorbed incident power distribution provided the best agreement between measured and simulated profiles. The magnitude of absorbed power in the volumetric heat source was adjusted in FEA in order to match model-derived equilibrium temperature distributions with temperature distributions measured by the infrared camera at steady-state. The magnitude of absorbed power was adjusted until resulting FEA equilibrium average temperature within a 1.2 mm region of interest centered on the heat source was within 0.1 °C of measured steady-state values.

III. Results & discussion

A. Large optical extinction per NP of AuNP in PVP films decreased with AuNP content

Subwavelength PVP films in which homogeneous 16 nm AuNP had been concentrated exhibited optical extinctions of up to 20% at thickness values of 70 ± 7 nm.[20] This was comparable to extinction from 130 nm thick polymer dispersions in which heterogeneous AuNPs had been reduced from gold salt solution.[36] However, the present work also used Maxwell-Garnett (EMT) and the coupled dipole approximation (CDA) to estimate optical extinction *a priori* to within 18 and 3% of measured values, respectively. EMT calculates a bulk dielectric function based on the constituent dielectric functions of the host media and inclusions which supports use of Fresnel optics to determine optical absorbance.[29,37] Resonant extinction per NP was defined to relate measured optical extinction to theoretical estimates. Measured and Maxwell Garnett EMT-derived extinction per NP was calculated as A/cnl, where A was measured or predicted absorbance (in absorbance units, AU) at 532 nm (the excitation wavelength for thermal measurements), c was concentration in NP per cm^3, n was refractive index (RI) of PVP (1.53), and l was film thickness in cm. The coupled dipole approximation (CDA) extends Mie particle polarizability to account for multiple particles and corresponding interparticle interactions.[23,24] Extinction per NP was calculated from CDA assuming a square particle lattice with interparticle separation distance estimated as double the Wigner–Seitz radius, $r_{W\text{–}S}$. The $r_{W\text{–}S}$ equals the mean spherical volume of medium per NP[38] and has been used to characterize interparticle distances between NP dispersed in condensed media.[12,31,39] Extinction magnitudes used for measured, EMT, and CDA values were calculated by difference from extinction measured at 800 nm (off-resonance).

Fig. 1 shows measured extinction per NP (right axis) in PVP (filled black squares) decreased overall as interparticle distance, $2 \times r_{W\text{–}S}$, decreased from 130 to 76 nm. *A priori* EMT values (hollow green diamonds) exhibited a similar, asymptotic decrease with magnitudes ranging from less than 1 to 5×10^{-13} cm^2 per NP greater than measured data. EMT estimates optical properties of nanocomposites to NP fill fractions of more than 0.1,[28] more than 10-fold greater than those herein. *A priori* CDA estimates of extinction per NP (hollow purple triangles) also decreased, from 9.62 to 9.51×10^{-13} cm^2 per NP, as interparticle separation decreased from 130 to 76 nm. Decreased interparticle spacing increases near-field interactions (*e.g.*, coupling and screening) and evolves plasmon polarization from dipole to multipole.[40] This diminishes optical extinction per NP as local field enhancement decreases. Interparticle spacings that approach NP size allow near-field coupling[41] which increases exchange of electromagnetic energy between NP and red-shifts the LSPR.[42] The observed downward trend at smaller interparticle distances reflected increased interactive coupling that suppressed resonant NP polarizability and resulting extinction.

Values of extinction per AuNP measured and simulated by EMT, Mie and CDA in Fig. 1 appeared relatively robust to possible variations in refractive index and film thickness. Values for extinction per NP in Fig. 1 were simulated using a refractive index ($n = 1.53$) slightly above that of glass ($n = 1.52$) to account for the thin PVP layer. This value for refractive index (RI) was used because reversing the orientation of the PVP film relative to incident light, *i.e.*, light incident on the PVP rather than the glass, changed neither measured LSPR energy nor

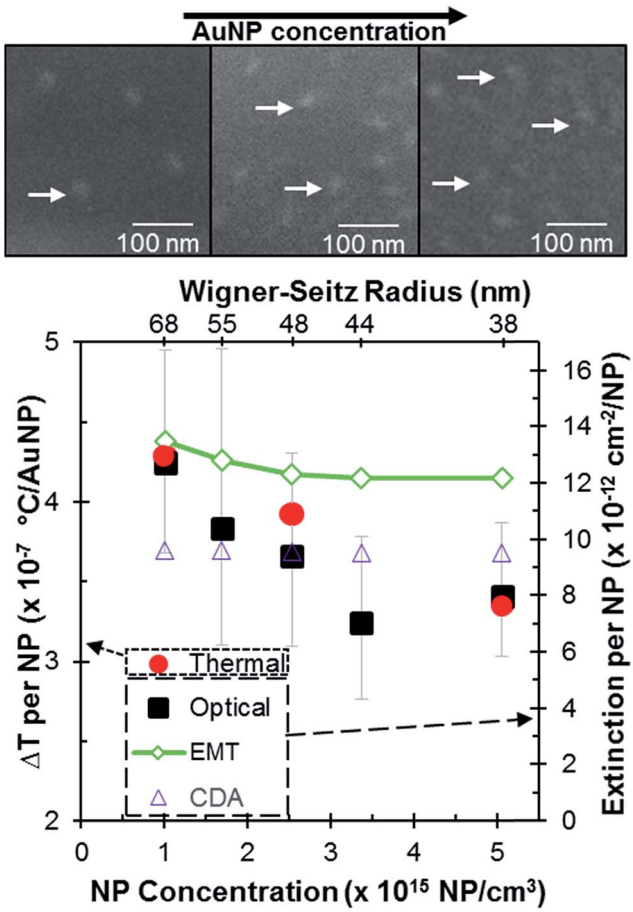

Fig. 1 Change in temperature per NP (red circles, left *y*-axis) with corresponding mean optical extinction per NP (right *y*-axis) for measured (black squares), Maxwell Garnett EMT (hollow green diamonds) and CDA (hollow purple triangles) taken at 532 nm for each AuNP–PVP film. High and low error in optical extinction per NP (black) and temperature change per NP, which were within the size of the shape for the latter, represent values derived from the maximum and minimum values of measured extinction magnitudes and thermal response, respectively. Upper inset shows representative 10 kV SEM images (normal incidence) of three AuNP–PVP films at consecutively larger AuNP content examined in the thermal analysis. Arrows identify individual AuNP.

amplitude. This appeared due to nearly identical refractive indices for PVP and glass. An alternative CDA simulation using effective RI of 1.3 for a 530 nm thick medium (*e.g.*, one wavelength thick) consisting of 70 nm of PVP, 230 nm of air (n = 1.00), and 230 nm of glass (n = 1.52) reduced extinction per NP by less than two-fold (relative to values in Fig. 1) as the LSPR wavelength blue-shifted from 540 nm to 525 nm due to diffractive coupling.[43] Measured values for extinction per NP in Fig. 1, calculated as absorbance divided by concentration, film thickness, and RI, would increase (decrease) by 11% (9%) at lower (upper) values of standard deviation of thickness measured for the PVP film: 70 ± 7 nm (N = 500). Charging effects and insufficient *z*-contrast precluded corroborating PVP thickness atop insulative 500 μm-thick BK-7 glass film using scanning electron microscopy (SEM) cross-sections (details in ESI†).

Trends and magnitudes of extinction per NP in Fig. 1 for PVP films containing 16 nm AuNP at the concentrations shown appeared similar between measured and simulated values, reflecting commonalities between the respective computational approaches. CDA simulated the randomly-dispersed AuNP in the 70 nm PVP films as a two-dimensional ordered lattice in order to gauge how much interparticle interactions (*e.g.*, near-field enhancement and far-field constructive phase interference) might dampen the decrease in extinction per NP as NP concentration increased in the film. It is expected that random perturbations to a regular lattice (*e.g.*, out-of-plane AuNPs in the actual PVP film) destructively interfere to decrease optical extinction relative to *a priori* CDA results, an effect that grows as particles become closer.[44–47] Thus, measured extinction per NP decreased relative to CDA simulations as AuNP content increased. CDA evaluates each isolated NP in a regular lattice as a scattering, polarizable point dipole onto which scattering contributions from neighboring NPs accrue in a retarded dipole sum.[23,24] Far-field diffraction dominates the retarded dipole sum when incident wavelength approaches interparticle spacing between ordered particles[33] in square[61] or triangular[62] configurations. Random perturbations to the regular lattice (*e.g.*, out-of-plane AuNPs) produce destructive interference to the retarded dipole sum in the CDA. This decreases the magnitude of optical extinction. Destructive interference due to disorder increases as particle separation decreases. Values of extinction measured for non-ordered AuNP in the fabricated PVP film decreased relative to *a priori* CDA simulations as AuNP content increased in Fig. 1, attributable to such destructive interference.

In the limit of zero interparticle interactions, calculated CDA polarizability converges to single particle Mie theory from which the cross-section of an isolated AuNP is calculable. The Mie approach underlies Beer–Lambert law for which absorbance increases linearly with concentration, a condition valid only for non-interacting NP.[12,48] Combining EMT and Mie theory to predict multipole interactions is unnecessary for 16 nm AuNP in the quasistatic regime, but could be required for more complex plasmonic nanostructures.[49] The utility of geometric optics for calculating absorbance in nm-thick films is limited by dominance of thin-film interference on optical properties.[50] Morphology-dependent optical responses[51] and increased absorption efficiency for plasmonic particles separations limited to twice NP diameter or less[52] have been examined using finite element analysis (FEA).

B. Temperature increases per NP and in the overall film

Resonant temperature increase per NP decreased with concentration for subwavelength PVP films containing 16 nm AuNPs at interparticle separations less than the incident wavelength. This matched trends in measured, Maxwell-Garnett, and CDA-derived values of optical extinction per NP. Fig. 1 compares the change in temperature per NP (ΔT per NP) (left axis) calculated as $\Delta T/NmC_p$ where ΔT is the change in temperature contribution from the NPs (*i.e.*, sample ΔT subtracted by ΔT of PVP control), N is the number of irradiated NPs, and mC_p is the

thermal mass of each sample. The number of irradiated NPs was calculated by multiplying the cylindrical volume of the 70 nm thick PVP film irradiated by the 1.2 mm diameter beam by NP concentration in NPs per cm^3. Change in temperature per NP was divided by thermal mass to correct for variations in total mass between samples with different concentrations of NP. Thus Fig. 1 plots the change in bulk temperature of the nanoparticle-embedded film change relative to the number of resonantly irradiated nanoparticles in the laser beam, not microKelvin temperature control of an isolated nanoparticle. The dynamic change and peak equilibrium change in bulk film temperature as a function of nanoparticle concentration are shown in Fig. S4(b) and S4(c),† respectively, in ESI.† A 7 nm change in film thickness (1 standard deviation) would change calculated values of both extinction/NP and ΔT per NP by −9 to +11%, giving different magnitudes for calculated values but yielding the same correspondence. Resulting temperature per NP values ranged from 4.29×10^{-7} °C per NP at 1.01×10^{15} NP per cm^3 to 1.93×10^{-7} °C per NP at an AuNP concentration of 3.37×10^{15} NP per cm^3. These results have important implications to design of photothermal devices: a sublinear increase in heat relative AuNP concentration in such systems yields a decreasing return.

Temperature increase per incident resonant power corrected for sample mass (°C g W^{-1}), including the glass substrate, from resonant absorption in subwavelength PVP films containing AuNP at particle separations much less than resonant wavelength, was comparable to prior work. The maximum °C g W^{-1} observed in this work, 3.2 for the 5.06×10^{15} NP per cm^3 AuNP–PVP film, was similar to values of *ca.* 3 for both AuNPs annealed on glass and fluid-filled capillaries.[13,15,16] This °C g W^{-1} was greater than an AuNP colloid solution[12,13] and PDMS films containing asymmetrically-distributed *in situ* reduced AuNPs.[53] Super-wavelength films exhibiting enhanced optical extinction at separations near the resonant wavelength have yielded the largest °C g W^{-1} of up to 19.[32] This comparison suggests layer-by-layer fabrication with control of spatial dimension and concentration could be implemented to enhance overall thermal response of PVP thin films containing Au nanostructures.[54,55] Effects of thermal mass are more completely accounted in Fig. 2.

Despite subwavelength optical confinement and high concentrations of NP with negligible Rayleigh scattering cross-sections, the measured thermal characteristics of these films conformed to a linear microscopic description. Overall magnitude of temperature increase in AuNP–PVP films irradiated at 532 nm laser scaled with AuNP concentration. Overall temperature increases may be explained *via* increased thermal coupling effects[56] at greater concentrations, giving rise to a delocalized heating regime[57] across the surface of the PVP film causing a larger overall temperature change for the system while contributing to the decrease in temperature change per NP. Dynamic thermal responses of the films yielded log-linear heating and cooling curves as expected from linear microscopic thermal analysis. Temperature increased logarithmically during laser excitation, approaching steady-state as the 90 second heating period ended. Subsequent cooling when irradiation ceased exhibited exponential decay. Example heating and cooling curves at each AuNP concentration are shown in Fig. S4 in ESI.† From these curves, thermal time constants were estimated to characterize dynamic thermal response[12] as well as photon-to-heat conversion. The small mass, high aspect ratio and significant local temperature increases in these samples rendered them susceptible to optothermal degradation.[56] Suppressed temperature increases in samples containing 3.37 and 1.69×10^{15} NP per cm^3 was attributed to laser induced damage (shown in ESI†). This excluded these samples from further analysis. SEM images showed 75–100 nm crater defects for the 3.37×10^{15} NP per cm^3 film inside the area under laser irradiation. Such defects were absent on the non-irradiated sample periphery.

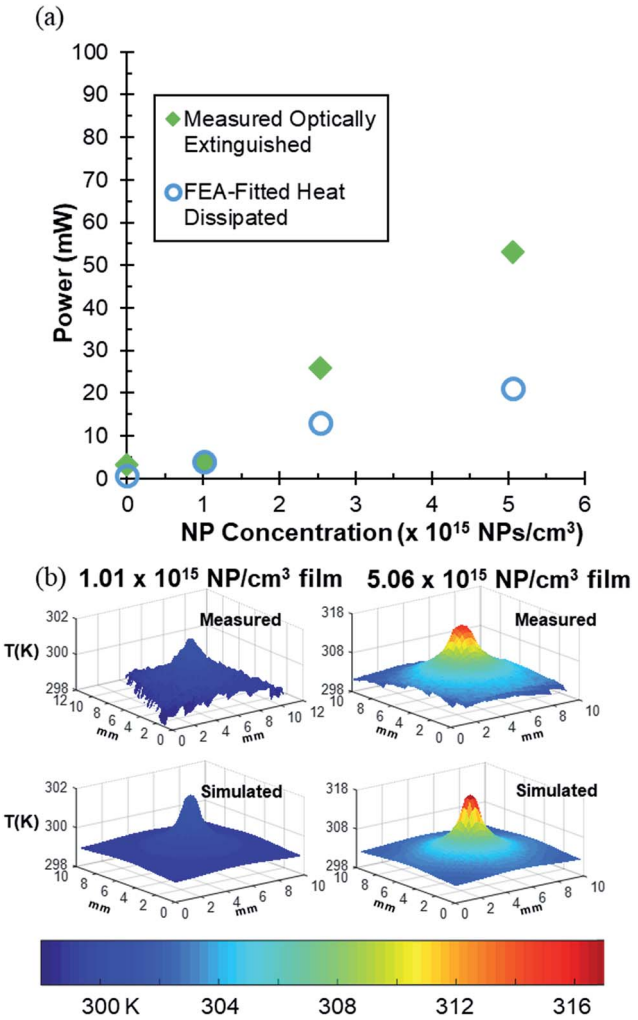

Fig. 2 (a) Optically extinguished power (filled green diamonds) and FEA-fitted dissipated thermal power based on measured temperature distribution (open blue circles) as a function of AuNP concentration. Error bars in both optically extinguished power and FEA-fitted heat dissipated power were within the size of the symbol. Error calculation is detailed in ESI.† (b) Comparison of measured and simulated thermal profiles for the 1.01 (LHS) and 5.06 (RHS) $\times 10^{15}$ NP per cm^3 films. Scheme 1 shows measured 1.01×10^{15} NP per cm^3 film has trapezoidal shape *vs.* square simulation.

C. Finite element analysis of heat dissipation

Trends and magnitudes of FEA estimates for power extinguished, heat flux, temperature distribution and thermal dynamics values based on published relations for convection, conduction, and radiation were consistent with values measured for subwavelength AuNP–PVP films. FEA estimates were produced using a simulation validated for thermal response in super-wavelength polymer films containing AuNPs at particle separations near or greater than LSPR wavelength.[31] Temperature distributions in respective AuNP–PVP films were simulated using a radially uniform volumetric heat source with a power that matched the value calculated from the measured optical extinction. Likewise, by iteratively matching measured and simulated temperature distributions, the heat source power could be estimated.

Fig. 2(a) shows measured values (filled green diamonds) of optically extinguished power in the AuNP–PVP films increased from 3.1 mW at 0.0 NP per cm^3 to 53.1 mW at 5.06×10^{15} NP per cm^3. Measured optically extinguished power was calculated by the relation[13] $(1 - 10^{-A_\lambda})I$ where I is the incident power and A_λ is the absorbance of AuNP–PVP at wavelength λ. Absorption for each sample was calculated at laser irradiation wavelength, 532 nm, with A_λ being determined by $A_\lambda = 2 - \log_{10}(T + R)$ where T and R were the transmission and reflectance of each sample measured at the given wavelength. Reflectance, measured independently in an integrating sphere, constituted 7% of incident power at 532 nm. Accounting for reflectance from the film improved accuracy of calculated AuNP–PVP absorption.[58] This is further detailed in the ESI.† The heat source power estimated by FEA (open blue circles) to be required to obtain an average temperature consistent with the average measured temperature in the laser spot was lower than measured power values by 2.31, 0.0611, 13.0, and 32.2 mW, respectively, for the films as AuNP content increased. FEA-calculated temperatures were fitted to observed temperature profiles by matching the average temperature of the 1.2 mm laser spot ROI within 0.1 °C of the measured value.

Topographic heat maps in Fig. 2(b) show measured temperature outside the laser spot exceeded temperature calculated using a Gaussian power source at the same location. The difference increased as AuNP density increased from 1.01 to 5.06×10^{15} NP per cm^3 film. This corresponded to increased underestimates from FEA of power requirement. Thus, matching average FEA-calculated and measured temperatures within the 1.2 mm laser spot to 0.1 °C resulted in (quantitative) qualitative agreement (within) outside the laser spot between measured and simulated temperature profiles. Two other fitting criteria yielded similar values for FEA-calculated power: the average temperature across the entire film was fit to within 0.1 °C between calculated and measured values; and by fitting estimates of thermally-dissipated power emitted, *via* radiation and convection, from the AuNP–PVP film face to corresponding values obtained by calculating radiation and convective from the measured temperature at each film pixel and summing over the entire film. Heat source power values derived from the latter two methods varied by *ca.* 5%, within the size of symbol in Fig. 2, from fits based on ROI temperature ranging from 0.0062 to 0.028 W.

Differences between simulated and observed powers in Fig. 2(a) appeared attributable primarily to increased optical/power dispersion apparent in measured samples. While average measured and simulated temperatures inside the laser spot were with 0.1 °C, calculated temperature distributions were narrower than measured profiles. Broader thermal profiles were likely to result in part from lateral optical dispersion observed previously at AuNP concentrations in which Wigner–Seitz separation decreased below resonant irradiation wavelength.[31] The volumetric heat source in the FEA model used to match the output from the diffuser did not include effect of lateral optical dispersion as a method to quantitate it has not yet been developed. Thermal dissipation in the FEA simulation appeared to be controlled overall by the thicker glass substrate rather than the 70 nm thick Au–PVP film in which the volumetric heat source was confined to simulate plasmonic absorption. Changes to PVP-layer thermal conductivity in the FEA model (*i.e.*, from $k = 0.27\ W\ mK^{-1}$, corresponding to pure PVP, to $3.2\ W\ mK^{-1}$, a mass-average between Au and PVP at 5.06×10^{15} NP per cm^3) had negligible effect on simulated temperature profiles.

Lower simulated heat dissipation could also have been a consequence of plasmonic saturation, edge effects, laser-induced damage or interfacial resistance in actual samples. Incident laser power of 800 mW used in this work have been shown to exhibit saturable absorption,[12] which was not included in the model. The microscale heat transfer coefficients used may have underpredicted heat transfer from the film's narrow vertical surfaces (~10 mm × ~0.5 mm). Heat transfer at nanometer-thick vertical surfaces may be underpredicted due to inward fluid flow induced near the edge of the plate, an effect previously reported to increase heat transfer rates up to two-fold.[59] This is not accounted for in the model. As a result, measured and modeled temperature values diverged near film edges. Evidence of laser induced damage to the sample, visible in the SEM images shown ESI,† may have suppressed the magnitude of measured thermal response in the laser spot. Interfacial resistance between PVP film and glass was not modeled.

To increase correspondence between FEA-simulated and measured thermal dissipation, quantitate methods to account for these effects could be developed and used to refine the simulations. Nevertheless, consistent overall trends in these initial comparisons between measured values of optically extinguished power and FEA-simulated values of power dissipation based on measured temperature profiles are an important first step to characterizing heat dissipation from plasmonic absorption in subwavelength films containing NP concentrated to separation distances much less than the resonant wavelength. The tools and systematic approach discussed here to characterize optical extinction and thermal dissipation in subwavelength AuNP films advance the ability to quantitatively identify a NP concentration and incident power that would yield a targeted temperature increase or steady power input for biomedical photothermal therapy[60] and drug delivery,[61] opto-mechanical systems,[62] or micro-etching.[62]

IV. Conclusion

This work examined heat dissipation due to optical extinction from resonant excitation of 16 nm AuNPs dispersed in 70 nm thick PVP films in comparison with *a priori* simulation of optical extinction and power dissipation, for the first time. Measured equilibrium temperature increase per NP decreased with AuNP concentration, matching the measured optical extinction per NP and corresponding to *a priori* Maxwell-Garnett effective medium theory, and coupled dipole approximation for optical extinction per NP. This showed plasmon heat dissipation per AuNP is limited as NP separation decreases at values less than the resonant wavelength. Heat dissipated per unit optical extinguished power and temperature distributions for AuNP–PVP thin films were simulated using a 3D finite element analysis that yielded trends and magnitudes comparable to optically extinguished power as AuNP content increased. Comparing measured and simulated optical and thermal values indicated the magnitude of possible effects due to lateral optical dispersion, plasmonic saturation, edge effects, and interfacial resistance to guide further examination. Demonstrating correspondence between measured and simulated optical and thermal responses of subwavelength nanoantenna-embedded polymer films identifies computational tools useful to advance rigorous design and adaptive control of nanocomposite films for application in energy, health and industrial processing.

Conflicts of interest

There are no conflicts of interest to declare.

Acknowledgements

This work was supported in part by NSF EEC-1260301 to D. Keith Roper, NSF REU grant awarded to Tyler V. Howard, NSF Graduate Research Fellowships awarded to Jeremy R. Dunklin and Gregory T. Forcherio, the University of Arkansas Foundation, and the Walton Family Charitable Foundation. Any opinions, findings, and conclusions or recommendations expressed in this material are those of the authors and do not necessarily reflect the views of the National Science Foundation. Tyler V. Howard setup thermal experiments, collected data, and prepared figures and text. Jeremy R. Dunklin fabricated samples, performed optical analysis, performed FEA modeling, and prepared manuscript text. Gregory T. Forcherio guided experimental set-up, performed SEM, and assisted in data analysis. D. Keith Roper conceived and directed the work and refined compilation of data, figures and text. The authors thank Timothy A. Morgan and Carter Bodinger for assistance with AFM to determine film thicknesses.

References

1 X. Jiang, R. Liu, P. Tang, W. Li, H. Zhong, Z. Zhou and J. Zhou, *RSC Adv.*, 2015, **5**, 80709–80718.
2 S. C. Dixon, W. J. Peveler, N. Noor, J. C. Bear and I. P. Parkin, *RSC Adv.*, 2016, **6**, 31146–31152.
3 X. Wu, Y. Gao and C.-M. Dong, *RSC Adv.*, 2015, **5**, 13787–13796.
4 A. Politano, A. Cupolillo, G. Di Profio, H. A. Arafat, G. Chiarello and E. Curcio, *J. Phys.: Condens. Matter*, 2016, **28**, 363003.
5 H. SadAbadi, S. Badilescu, M. Packirisamy and R. Wüthrich, *Biosens. Bioelectron.*, 2013, **44**, 77–84.
6 J. Poursafar, M. Kolahdouz, E. Asl-Soleimani and S. Golmohammadi, *RSC Adv.*, 2016, **6**, 55354–55359.
7 D. Wenting, K. Saleem, L. Leandro, V. Vincenzo and D. Ravinder, in *2015 11th Conference on Ph.D. Research in Microelectronics and Electronics (PRIME)*, IEEE, Glasgow, UK, 2015.
8 G. Mie, *Ann. Phys.*, 1908, **330**, 377–445.
9 C. F. Bohren and D. R. Huffman, *Absorption and Scattering of Light By Small Particles*, Wiley, New York, NY, 1998.
10 S. Berciaud, L. Cognet, P. Tamarat and B. Lounis, *Nano Lett.*, 2005, **5**, 515–518.
11 K. C. Grabar, R. G. Freeman, M. B. Hommer and M. J. Natan, *Anal. Chem.*, 1995, **67**, 735–743.
12 D. K. Roper, W. Ahn and M. Hoepfner, *J. Phys. Chem. C*, 2007, **111**, 3636–3641.
13 W. Ahn and D. K. Roper, *J. Phys. Chem. C*, 2008, **112**, 12214–12218.
14 K. R. Berry, A. G. Russell, P. T. Blake and D. K. Roper, *Nanotechnology*, 2012, **23**, 11.
15 A. G. Russell, M. D. McKnight, A. C. Sharp, J. A. Hestekin and D. K. Roper, *J. Phys. Chem. C*, 2010, **114**, 10132–10139.
16 A. G. Russell, M. D. McKnight, J. A. Hestekin and D. K. Roper, *Langmuir*, 2011, **27**, 7799–7805.
17 K. R. Berry, J. R. Dunklin, P. A. Blake and D. K. Roper, *J. Phys. Chem. C*, 2015, **119**, 10550–10557.
18 S. Link, Z. L. Wang and M. A. El-Sayed, *J. Phys. Chem. B*, 2000, **104**, 7867–7870.
19 H. H. Richardson, Z. N. Hickman, A. O. Govorov, A. C. Thomas, W. Zhang and M. E. Kordesch, *Nano Lett.*, 2006, **6**, 783–788.
20 J. R. Dunklin, C. Bodinger, G. T. Forcherio and D. K. Roper, *J. Nanophotonics*, 2017, **11**, 16002.
21 G. A. Rance, D. H. Marsh and A. N. Khlobystov, *Chem. Phys. Lett.*, 2008, **460**, 230–236.
22 S. Kubo, A. Diaz, Y. Tang, T. S. Mayer, I. C. Khoo and T. E. Mallouk, *Nano Lett.*, 2007, **7**, 3418–3423.
23 E. M. Purcell and C. R. Pennypacker, *Astrophys. J.*, 1973, **186**, 705–714.
24 B. T. Draine and P. J. Flatau, *J. Opt. Soc. Am. A*, 1994, **11**, 1491–1499.
25 S. K. Ghosh and T. Pal, *Chem. Rev.*, 2007, **107**, 4797–4862.
26 J. C. Maxwell and B. A. Garnett, *Philos. Trans. R. Soc., A*, 1904, **203**, 359–371.
27 O. Levy and D. Stroud, *Phys. Rev. B: Condens. Matter Mater. Phys.*, 1997, **56**, 8035–8046.
28 C.-A. Guérin, P. Mallet and A. Sentenac, *J. Opt. Soc. Am. A*, 2006, **23**, 349–358.
29 G. A. Niklasson, C. G. Granqvist and O. Hunderi, *Appl. Opt.*, 1981, **20**, 26–30.

30 A. G. Russell, M. D. McKnight, J. A. Hestekin and D. K. Roper, *Langmuir*, 2011, **27**(12), 7799–7805.
31 J. R. Dunklin, G. T. Forcherio, K. R. Berry and D. K. Roper, *J. Phys. Chem. C*, 2014, **118**, 7523–7531.
32 J. R. Dunklin and D. K. Roper, *J. Nanomater.*, 2017, **2017**, 2753934.
33 D. K. Roper, W. Ahn, B. Taylor and Y. D'Asen, *IEEE Sens. J.*, 2010, **10**, 531–540.
34 L. De Sio, T. Placido, R. Comparelli, M. Lucia Curri, M. Striccoli, N. Tabiryan and T. J. Bunning, *Prog. Quantum Electron.*, 2015, **41**, 23–70.
35 H. Ebadi-Dehaghani and M. Nazempour, in *Smart Nanoparticles Technology*, ed. A. Hashim, 2012, pp. 519–534.
36 R. Abargues, K. Abderrafi, E. Pedrueza, R. Gradess, J. Marqués-Hueso, J. L. Valdés and J. Martínez-Pastor, *New J. Chem.*, 2009, **33**, 1720.
37 J. C. Maxwell Garnett, *Philos. Trans. R. Soc., A*, 1904, **203**, 385–420.
38 L. A. Girifalco, *Statistical Mechanics of Solids*, Oxford University Press, USA, 2000.
39 J. R. Dunklin, G. T. Forcherio and D. Keith Roper, *Mater. Res. Express*, 2015, **2**, 85005.
40 T. Atay, J. H. Song and A. V. Nurmikko, *Nano Lett.*, 2004, **4**, 1627–1631.
41 R. G. Hobbs, Y. Yang, A. Fallahi, P. D. Keathley, E. De Leo, F. X. Kartner, W. S. Graves and K. K. Berggren, *ACS Nano*, 2014, **8**, 11474–11482.
42 K. H. Su, Q. H. Wei, X. Zhang, J. J. Mock, D. R. Smith and S. Schultz, *Nano Lett.*, 2003, **3**, 1087–1090.
43 P. Blake, S. Kühne, G. T. Forcherio and D. K. Roper, *J. Nanophotonics*, 2014, **8**, 83084.
44 J. C. Norman, D. F. DeJarnette and D. K. Roper, *J. Phys. Chem. C*, 2014, **118**, 627–634.
45 D. Dejarnette, J. Norman and D. K. Roper, *Appl. Phys. Lett.*, 2012, **101**, 2010–2015.
46 D. DeJarnette, D. K. Roper and B. Harbin, *J. Opt. Soc. Am. B*, 2012, **29**, 88.
47 D. K. Roper, W. Ahn, B. Taylor and A. G. D. Asen, *IEEE Sens. J.*, 2010, **10**, 531–540.
48 R. M. Bright, M. D. Musick and M. J. Natan, *Langmuir*, 1998, **14**(20), 5695–5701.
49 A. Malasi, R. Kalyanaraman and H. Garcia, *J. Opt.*, 2014, **16**, 65001.
50 M. A. Kats, R. Blanchard, S. Ramanathan and F. Capasso, *Opt. Photonics News*, 2014, **25**, 40–47.
51 A. M. Kern and O. J. F. Martin, *Proc. SPIE*, 2009, **7395**, 739518.
52 N. Zeng and A. B. Murphy, *Nanotechnology*, 2009, **20**, 375702.
53 J. R. Dunklin, G. T. Forcherio, K. R. Berry and D. K. Roper, *ACS Appl. Mater. Interfaces*, 2013, **5**, 8457–8466.
54 J. T. O'Neal, M. J. Bolen, E. Y. Dai and J. L. Lutkenhaus, *J. Colloid Interface Sci.*, 2017, **485**, 260–268.
55 M. Lisunova, J. R. Dunklin, S. V. Jenkins, J. Chen and D. K. Roper, *RSC Adv.*, 2015, **5**, 15719–15727.
56 A. O. Govorov, W. Zhang, T. Skeini, H. Richardson, J. Lee and N. A. Kotov, *Nanoscale Res. Lett.*, 2006, **1**, 84–90.
57 G. Baffou, P. Berto, E. Bermúdez Ureña, R. Quidant, S. Monneret, J. Polleux and H. Rigneault, *ACS Nano*, 2013, **7**, 6478–6488.
58 G. T. Forcherio and D. K. Roper, *Appl. Opt.*, 2013, **53**, 6417–6427.
59 P. H. Oosthuizen and A. Y. Kalendar, Natural Convective Heat Transfer from Narrow Plates in *Thermal Engineering and Applied Science*, Springer Briefs, 2013, DOI: 10.1007/978-1-4614-5158-7_2.
60 X. Huang and M. A. El-Sayed, *J. Adv. Res.*, 2010, **1**, 13–28.
61 P. Thoniyot, M. J. Tan, A. A. Karim, D. J. Young and X. J. Loh, *Adv. Sci.*, 2015, **2**, 1–13.
62 R. Pimentel-Dominguez, A. M. Velazquez-Benitez, J. R. Velez-Cordero, M. Hautefeuille, F. Sanchez-Arevalo and J. Hernandez-Cordero, *Polymers*, 2016, **8**(4), 84, DOI: 10.3390/polym8040084.